CHAPTER 3

EXPERIMENTAL WORK

The present chapter describes the synthesis of $Fe_{(100-x)}Ni_{(x)}$ alloy and (Fe-Ni)-ZrO_2 composite specimens and their characterization using various techniques. A flow chart showing synthesis and characterization is shown in Fig. 3.1.

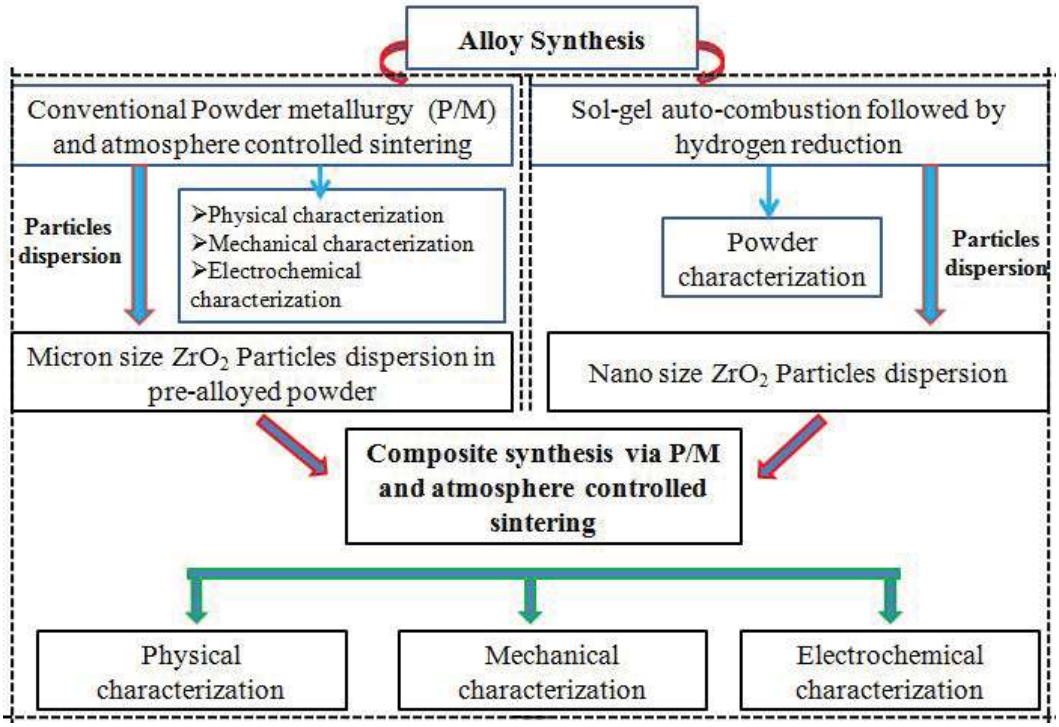

FIGURE 3.1: Flow diagram for synthesis and Characterization of Fe-Ni alloys and (Fe-Ni)-ZrO_2 composite specimens.

Different $Fe_{(100-x)}Ni_{(x)}$ alloy specimens (where Ni varies from 10 to 50 wt.%) have been prepared via solid-state reaction route (powder metallurgy P/M) and chemical synthesis (sol-gel auto-combustion followed by the reduction in hydrogen atmosphere). The study of phase, mechanical and corrosion behavior of prepared alloy specimens was done.

TABLE 3.1: Characteristics of chemicals used.

S.No.	Powder	Supplier	Characteristics
1	Fe	Loba Chemie	250-300μm 99.5% purity
2	Ni	Loba Chemie	74μm and 99.5% purity
3	ZrO_2	Loba Chemie	11-39μm and 99.8% purity

Alloy composition $Fe_{70}Ni_{30}$ was selected for composite synthesis. The synthesis of the composite was done by addition of hard ZrO_2 particles (0, 2.5, 5, 10 and 15 wt.%) in the selected alloy composition. Micro and nano-size ZrO_2 particles were added in the mechanically mixed and chemically prepared alloy powders, respectively. Composite fabrication from the mixed powders was done using powder metallurgy route. Powder metallurgy P/M processing technique is extensively used for the preparation of specimens for structural, mechanical and electrochemical characterization.

3.1 Synthesis of $Fe_{(100-x)}Ni_{(x)}$ Alloys and $(Fe_{70}Ni_{30})$-ZrO_2 Composite Specimens via Powder Metallurgy Route

The important steps during $Fe_{(100-x)}Ni_{(x)}$ alloy and composite synthesis via powder metallurgy route is as follows:

3.1.1 Materials selection

Synthesis of $Fe_{(100-x)}Ni_{(x)}$ alloy and ZrO_2 reinforced composites include the selection of materials first. The characteristics of chemicals used for material synthesis is given in Table 3.1.

Table 3.2 shows the compositions selected for the fabrication of alloy specimens. For

TABLE 3.2: Composition and nomenclatures used for $Fe_{(100-x)}Ni_{(x)}$ alloy specimens.

S.No.	Fe (wt.%)	Ni (wt.%)	Nomenclature
1	90	10	$Fe_{90}Ni_{10}$
2	80	20	$Fe_{80}Ni_{20}$
3	70	30	$Fe_{70}Ni_{30}$
4	60	40	$Fe_{60}Ni_{40}$
5	50	50	$Fe_{50}Ni_{50}$

TABLE 3.3: Composition and nomenclature used for $(Fe_{70}Ni_{30})$-ZrO_2 composites.

S.No.	Fe (wt.%)	Ni (wt.%)	ZrO_2 (wt.%)	Nomenclature
1	70	30	0	$(Fe_{70}Ni_{30})$
2	68.25	29.25	2.5	$(Fe_{70}Ni_{30})$-$2.5ZrO_2$
3	66.5	28.5	5	$(Fe_{70}Ni_{30})$-$5ZrO_2$
4	63.0	27.0	10	$(Fe_{70}Ni_{30})$-$10ZrO_2$
5	59.5	25.5	15	$(Fe_{70}Ni_{30})$-$15ZrO_2$

convenience, the nomenclature is given for each composition. For example, $Fe_{90}Ni_{10}$ represents the composition containing 90 wt.% Fe and 10 wt.% Ni. Table 3.3 shows the composition and nomenclature used for the composite specimens. For example, $(Fe_{70}Ni_{30})$-$2.5ZrO_2$ represents the composition containing 2.5 wt.% ZrO_2 as reinforcement particles from the total 100 wt.% mass. Remaining 97.5 wt.% mass consists of the metal matrix (70 wt.% Fe and 30 wt.% Ni) i.e., the relative fraction of Fe and Ni in different composite specimens remain constant.

3.1.2 Weighing and Milling

Depending on the composition, calculated amounts of chemicals such as iron, nickel, and zirconia were weighed accurately using an electronic balance having an accuracy of 0.0001 gm. The name and amount of chemicals are listed in Table 3.1, Table 3.2 and Table 3.3. These powders were mixed vigorously using a centrifugal ball mill (Retsch, S1

Germany) in dry medium. Zirconia balls were added as grinding media for better mixing, where powder to ball ratio was kept 1:2 (in weight ratio). Dextrine was used as a binder ($\sim$1wt.%) during milling to provide green strength to specimens during compaction. The ball milling was done at a speed of 200 rpm for 2h. The final powder contains a homogenous mixture of all the added powders.

3.1.3 Compaction

Compaction of the homogenous powder mix was done using a uniaxial hydraulic press. For compaction a high chrome high carbon steel die of 12.9 mm diameter was used. It was observed that 120 kN load was giving the maximum green density of the compacts. Therefore, all the specimens were compacted at the same load to attain cylindrical shapes. Green alloy (h$\sim$20 mm and d$\sim$12.9 mm) and composite (h$\sim$14.5mm and d$\sim$12.9 mm) specimens were obtained in cylindrical shapes.

3.1.4 Sintering

Green specimens were sintered in argon atmosphere using an atmosphere controlled tube furnace. For all the specimens, the heating rate was kept at a fixed rate, i.e., 5°C/min to reach 500°C. The furnace was held for 1 h for the removal of binder. The temperature was again increased from 500°C to sintering temperature at the same heating rate. For alloy specimens, the sintering was done at three different temperatures, i.e., 1000, 1200 and 1250°C for 1h. For composites, the sintering was done at 1150°C for 3h. The sintering

schedule of both alloys and composites is shown in Fig. 3.2 and Fig. 3.3. The prepared cylindrical specimens are shown in Fig. 3.4.

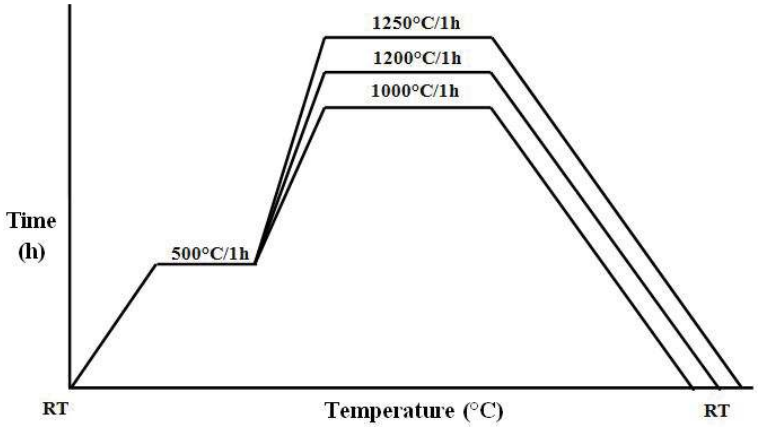

FIGURE 3.2: Sintering schedule for alloy specimens.

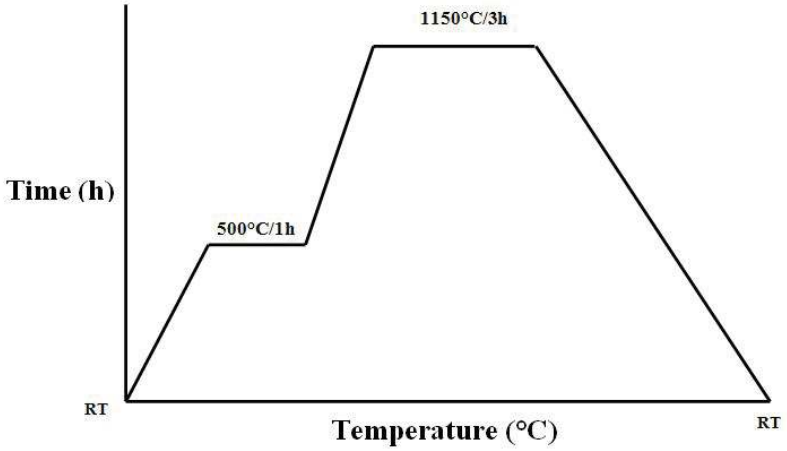

FIGURE 3.3: Sintering schedule for composite specimen.

FIGURE 3.4: Digital pictographs of cylindrical compacts.

3.2 Synthesis of Nanocrystalline $Fe_{(100-x)}Ni_{(x)}$ Alloy powder via Wet Chemical Route and Synthesis of ZrO_2 Nanoparticles Dispersed Metal Matrix Composite via Powder Metallurgy Route

3.2.1 Alloy powder synthesis

Auto-combustion synthesis route followed by reduction was adapted for synthesizing $Fe_{(100-x)}Ni_{(x)}$ (x=10, 30 and 50 mole%) alloy nano powders [81]. Stoichiometric amount of $Fe(NO_3)_3$. $9H_2O$ and $Ni(NO_3)_2.6H_2O$ were used as starting materials as a source of Fe and Ni respectively. Table 3.4 shows the characteristics of chemicals used in the powder synthesis. The nomenclature and compositions used for synthesizing alloy powders is listed in Table 3.5. Citric acid was used as a fuel and citrate to nitrate ratio (C/N) equal to 0.3 was maintained based on the previous literature for controlled combustion [92,93]. All chemicals of analytical reagent grade were weighed accurately and dissolved in minimum amount of de-ionized water separately. The amount of chemicals used during synthesis are listed in Table 3.6. These transparent solutions were mixed using a magnetic stirrer. The mixed solution was then heated at 95°C on a hot plate with continuous stirring. Water was evaporated, and solution converted into a thick gel. Further heating resulted in the swelling of gel followed by its auto-combustion with yellow flame producing a very fine

powder. This powder was then ground and reduced in the controlled atmosphere furnace with flowing hydrogen at 700°C for 1h.

After confirming the phase formation in synthesized nanopowders, powder metallurgy route was used for synthesizing composite specimens. The schematic diagram for $Fe_{(100-x)}$ $Ni_{(x)}$ alloy powder synthesis is shown in Fig. 3.5.

TABLE 3.4: Characteristics of chemicals used for auto-combustion.

S.No.	Powder	Supplier	Characteristics
1	$Fe(NO_3)_3.9H_2O$	Loba Chemie	98% purity
2	$Ni(NO_3)_2.6H_2O$	Loba Chemie	99% purity
3	$C_6H_8O_7$	Loba Chemie	99.5% purity

TABLE 3.5: Composition and nomenclatures used for chemically synthesized $Fe_{(100-x)}Ni_{(x)}$ alloy powders.

S.No.	Fe (mole%)	Ni (mole%)	Nomenclature
1	90	10	A-($Fe_{90}Ni_{10}$)
3	70	30	A-($Fe_{70}Ni_{30}$)
5	50	50	A-($Fe_{50}Ni_{50}$)

TABLE 3.6: Amount of chemicals used for synthesis for different alloy powders.

S.No.	Composition	$Fe(NO_3)_3.9H_2O$ (gm)	$Ni(NO_3)_2.6H_2O$ (gm)	Citric acid (gm)
1	A-($Fe_{90}Ni_{10}$)	66.10	5.23	29.92
2	A-($Fe_{70}Ni_{30}$)	50.90	15.54	27.58
3	A-($Fe_{50}Ni_{50}$)	35.99	25.64	25.29

3.2.2 Composite synthesis

3.2.2.1 Weighing and mixing

The synthesized alloy powder and nano zirconia powder were used in a required proportion as starting materials for composite preparation. Nomenclature and composition of

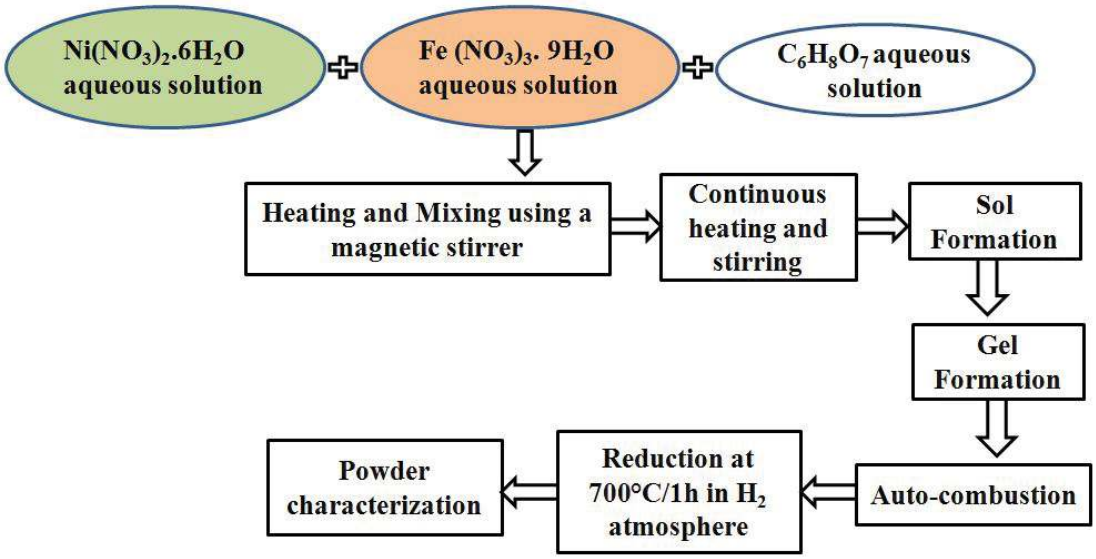

FIGURE 3.5: Flow diagram of alloy powder synthesis via wet chemical route.

TABLE 3.7: Nomenclatures used for nano ZrO_2 particles reinforced (Fe-Ni)-ZrO_2 composites.

S.No.	Nomenclature	$Fe_{70}Ni_{30}$ (wt.%)	ZrO_2(wt.%) (60-80nm), Lobachemie, 99.9%pure
1	A- ($Fe_{70}Ni_{30}$)	100	0
2	A-($Fe_{70}Ni_{30}$)-2.5ZrO_2	97.5	2.5
3	A-($Fe_{70}Ni_{30}$)-5ZrO_2	95	5
3	A-($Fe_{70}Ni_{30}$)-10ZrO_2	90	10
3	A-($Fe_{70}Ni_{30}$)-5ZrO_2	85	15

each specimen are listed in Table 3.7. The powders were weighed using an electronic balance having an accuracy of 0.0001 gm. Weighed powders were mixed using an agate mortar (1h) for homogenous mixing.

3.2.2.2 Compaction

The uniform powder mix was pressed in pellet form at a load 120 kN using an uniaxial hydraulic press. The compacts have the dimension h∼3-4 mm and d∼12.9 mm. Compacted specimens are shown in Fig. 3.6.

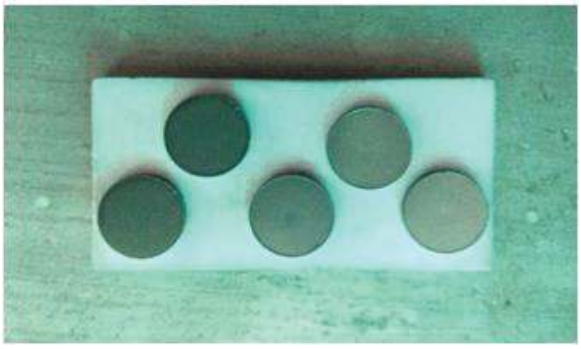

FIGURE 3.6: Digital pictographs of compact pellets.

3.2.2.3 Sintering

Green specimens were sintered in 95%Ar+5%H_2 atmosphere using an atmosphere controlled tube furnace. All the pellets were sintered at 900°C/1h at a heating rate 5°C/min The sintering schedule is shown in Fig. 3.7. The well polished sintered specimens can be seen in Fig. 3.8

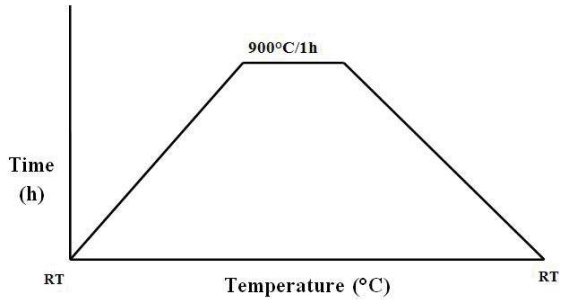

FIGURE 3.7: Sintering schedule for composite specimen.

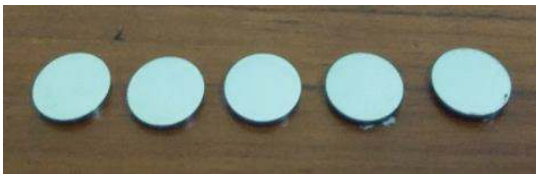

FIGURE 3.8: Digital pictographs of sintered pellets after polishing.

3.3 Characterization Techniques

Different characterization techniques used for the sintered alloy and composite specimens are listed in Fig. 3.9

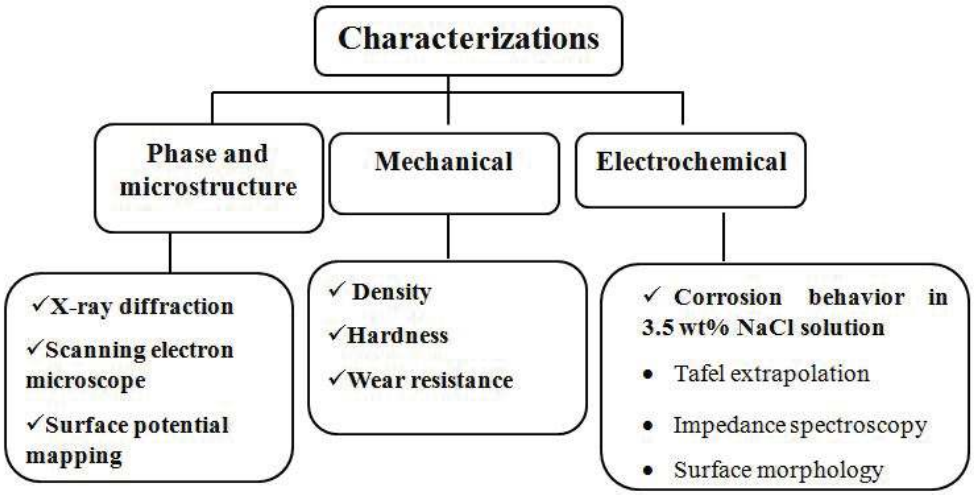

FIGURE 3.9: Different characterizations techniques used.

3.3.1 X-ray Diffraction (XRD)

X-ray diffraction is a non destructive method, used for determining the crystal structure of given material. It is used to analyze the phase, structure, imperfections and quantitative analysis. The constructive interference in a particular direction results by the interaction of X-rays reflected by a set of parallel planes satisfying Bragg's condition [94, 95]. The Bragg equation for diffraction can be represented as: $n\lambda = 2d\ Sin\theta$, where λ is the wavelength of X-rays, 'θ ' is the glancing angle (called as Bragg's angle), 'd' is the inter-planar separations and n is the order of diffraction, and it is taken as 1. The XRD data provide

the intensity/counts per second (cps), which is recorded by the detector as a function of 2θ, where θ is the angle of incidence [96].

Phase determination of all the samples was carried out using Rigaku mini flex 600 X-ray diffractometer. Analysis of obtained pattern was done with the help of X pert high score software using standard JCPDS files. The crystallite size (D) of A-($Fe_{(100-x)}Ni_{(x)}$) alloy powders obtained by wet chemical route was calculated using the Scherrer formula: D = 0.9λ / β Cosθ, where λ is the wavelength of X-ray, β is the full width at half maxima, and θ is the angle of diffraction.

3.3.2 Scanning Electron Microscopy (SEM)

Scanning electron microscope is used to obtain the surface morphology of a sample at different magnifications, resolution, and depth of focus. The images are taken at a higher resolution as compared to the optical microscope. A well-focused mono energetic electron beam is incident on the given solid surface. The interaction between beam and surface results in different scattering processes. Secondary electrons (SE) and back scattered electrons (BSE) are mainly used in SEM technique to get the surface morphology. These BSE or SE are collected and converted into current signals which are amplified to control the brightness of the cathode ray tube (CRT)/screen of monitor [97, 98]. SEM works in vacuum conditions. Therefore, special sample preparation is required before putting the samples for imaging. No moisture content should be there in the sample or the chamber because it would inhibit the vacuum in the chamber. Since the sample should be conducting in nature, therefore, metals do not need any preparation before being used. In

the present study, as prepared samples were ground for flat finish using different grade emery papers (1/0, 2/0, 3/0 and 4/0). The ground surface was polished using 0.5 μm diamond suspension. After polishing, the samples were ultrasonicated in acetone medium for almost 5 minutes to remove the impurities from the surface. The SEM images of a well-polished surface of as-prepared samples were taken in back scattered mode. A few samples were etched with 2% Nital solution before taking microstructure images at higher magnifications. These well-polished surfaces were used for the wear test. For corrosion test, specimens were cut in 2.5-3 mm height using the diamond saw cutter and then polished well. The worn and corroded sample surfaces were cleaned and dried before SEM examination. EDX and mapping were recorded at specific magnification to get the elemental analysis of as prepared and corroded surfaces. Microstructure study was carried out with the help of Evo18 Zeiss Scanning Electron Microscope (SEM), equipped with energy dispersive spectroscopy (EDX) system.

3.3.3 Density

Green density measurement of the compacted specimens was carried out using the formula: D= m/V= m/(π r^2h) where D is the density of the specimen in the green state, m is mass, r is the radius, h is the height and V is the volume of the green specimen after compaction. The density of sintered specimens was determined by Archimedes principle using the formula: W_d / (W_a-W_s), where W_d is weight of the dry sample, W_s is suspended weight and W_a is the soaked weight of sample.

3.3.4 Hardness

Hardness is a surface property, which provides the ability to resist against permanent deformation such as break, bent or any other deformation against externally applied load on any material [99]. It can also be defined as the resistance against indentation, penetration, and abrasion. When an external force is applied, the material shows some resistance and this resistance against permanent shape change is known as hardness. From the 'Metals Handbook,' hardness is defined as "Resistance of a metal to plastic deformation, usually by indentation." However, the term may also refer to stiffness or temper or resistance to scratching, abrasion, or cutting. The high hardness of the metal shows high resistance to deformation.

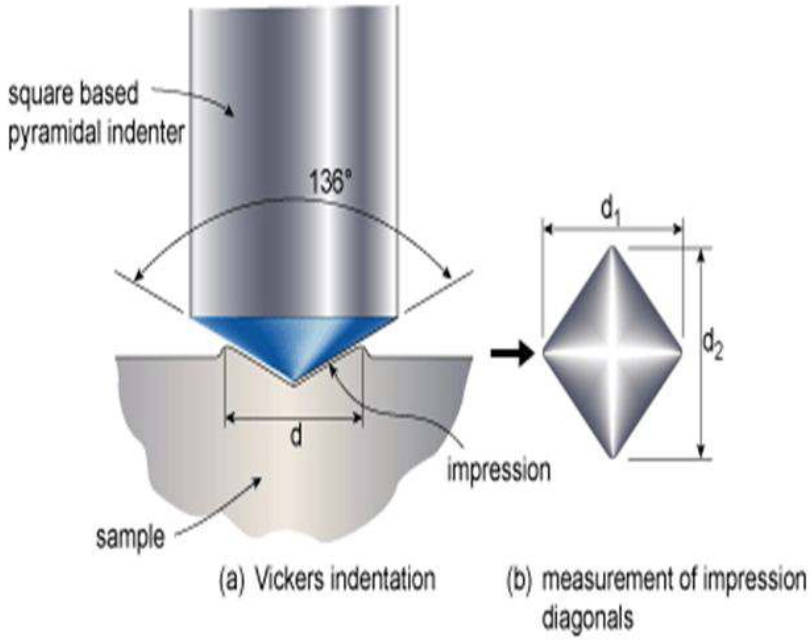

FIGURE 3.10: Vicker's hardness technique used for hardness measurement [100].

Different methods such as Shore Hardness Test, Barcol's hardness test, Rockwell

Hardness Test, Brinell Hardness, Knoop Hardness Test, Microhardness test and Vickers Hardness Test are commonly used for the measurement of the hardness worldwide. Fig. 3.10 shows the schematic of Vickers hardness measurement technique used in the present investigation.

Vickers Hardness Test is the standard method used for measuring the hardness of metals, particularly those with extremely hard surfaces. Vickers hardness is a measure of the hardness of a material, calculated from the size of an impression produced, under a load by a pyramid-shaped diamond indenter. The indenter employed in the Vickers test is a square-based pyramid whose opposite sides meet at the apex at an angle of 136°. In this test, the surface is subjected to a standard load for a standard length of time through an indenter. The diagonal of the resulting indentation is measured under a microscope, and the Vickers Hardness value read from a conversion table [101]. The Vickers number (H_V) is calculated using the following formula: $H_V = 1.854(F/d^2)$ where F is applied load (kgf) and d^2 is the area of indentation (mm^2). In the present work, Vickers hardness was measured by a Leco- LV700AT hardness tester under a load 5 kgf, applied for 10 sec. The average of 5 indentations was taken for each specimen.

3.3.5 Wear

Wear is known as the erosion, deformation or gradual deformation on a solid surface. It is the sideways displacement of a material from its original position on a solid surface which is performed by sliding one on another surface. Wear is the interaction between two surfaces and more particularly the removal of material from a surface resulting from a

mechanical action of the opposite surfaces. The relative motion between both surfaces and also the initial contact between asperities is the important difference between mechanical wear as compared to other similar processes [102].

The description of wear includes the loss of material from plastic deformation, if it originates between two surfaces sliding on each other. On the other hand, plastic deformation like yield stress can be excluded from the wear definition, because there is no relative sliding motion or contact between the surfaces. Impact wear is a sliding motion, which includes the interaction of two solid surfaces at an exceptionally short time interval. Earlier, the contact in impact wear was referred as the impulse wear. It can be explained as a mathematical model of the average of energy transport between two moving solids, which are in opposite converging contact [103].

1. Stages of Wear

Under normal conditions, there may be three stages of wear-rate of a material [104]:

(i) Primary stage which is also known as 'early run-in period'. In this stage, wear rate may vary from low to high and surfaces adapt to each other.

(ii) Secondary stage which is also known as a mid-age process. In this stage, a steady rate of aging is in motion.

(iii) Tertiary stage which is also known as the old-age period in which the rapid failure of material results due to high aging rate. Wear rate also depends on the processing and operating conditions. The secondary stage is reduced with the severe change in environmental conditions (higher temperatures, sliding velocities, strain rates, stress, etc.). Normal applied load and sliding speed are the significant parameters in altering the wear

rate. With this, 'tribo-chemical reaction' is also a significant term to understand the wear properties. During sliding, the formation of oxide layers occurs between the sliding surfaces. The formation of layers occurs due to the complex interaction between the surfaces, lubricants or environmental molecules.

2. Types of Wear

The study of wear is the part of tribology. The complex nature of wear results in different wear mechanisms. Some common wear processes are as follows: [105].

Adhesive wear: Adhesive wear occurs during frictional contact between surfaces. The unwanted displacement or attachment of wear debris occurs from one surface to another during the process. Usually, two surfaces slide over each other under some normal applied load in adhesive wear mechanism. This can be explained as plastic deformation within the small fragment surface layers. The severity of mechanism can be defined by the roughness, unevenness or the particles removal from the surface during application. These particles may attach to another surface due to strong adhesive forces of atoms and due to the energy accumulation in the plastic zone between the asperities.

Abrasive wear: Abrasive wear becomes prominent when a hard, rough surface slides opposite to a softer surface. From the ASTM International (formerly American Society for Testing and Materials) definition, abrasive wear causes the loss of material due to hard particles, forced against a moving solid surface. It is generally classified according to the type of contact and environment. The mode of abrasive wear can be determined by the kind of contact. There are two conventional modes of abrasive wear, which are two-body and three-body abrasive wear. Two-body wear occurs when hard particles remove

the material from the opposite surface. The typical correlation is the material removal by cutting or plowing operation. Three-body wear mechanism occurs when the particles are free to roll and slide down a surface. The contact environment determines the classification (whether the wear is open or closed). An open contact environment occurs, when the surfaces are sufficiently displaced and become independent of one another.

Surface fatigue: It is defined as a process by which the surface of a material is destabilized due to cyclic loading. This is a kind of material fatigue. It is created, when the wear particles are separated by cyclic crack growth, resulting from the micro cracks of the surface. These micro cracks may be either superficial or subsurface.

Fretting wear: It is the repeated cyclical rubbing between two surfaces over a period, which removes the material from one or both surfaces in contact depending upon the comparative hardness of both. Fretting wear occurs typically in bearings, although most bearings have their surfaces hardened to defend against the problem. Another problem arises when cracks are created on either surface. This is the more severe phenomenon among two, which can lead to catastrophic failure of bearing. The small particles removed due to the wear action may get oxidized in air and can also cause the wear enhancement because these oxides are usually harder than the parent metal. This may accelerate the wear loss as the harder particles abrade the metal surfaces. This is similar to the fretting corrosion in the presence of water. This mechanism can be seen in the unprotected bearings on large structures. For example, the severe degradation in bridges can be observed, when the salt is used during winter to unfreeze the highways.

Erosive wear: This can be defined as an extremely short sliding motion performed

for a very short duration which is a commonly encountered mechanism in industries. It is caused due to the impact of solid/liquid particles against the specimen surface. The impact of these particles results in the material removal due to repeated deformation. The slurry movement from piping and pumping equipment is a typical example of erosive wear.

The wear rate may depend upon several factors such as hardness, shape and impact velocity of the material.

3. Determination of Wear using Pin on Disc Wear and Friction Testing Machine

Fig. 3.11 shows schematic of a pin on disc wear testing machine. The system consists of

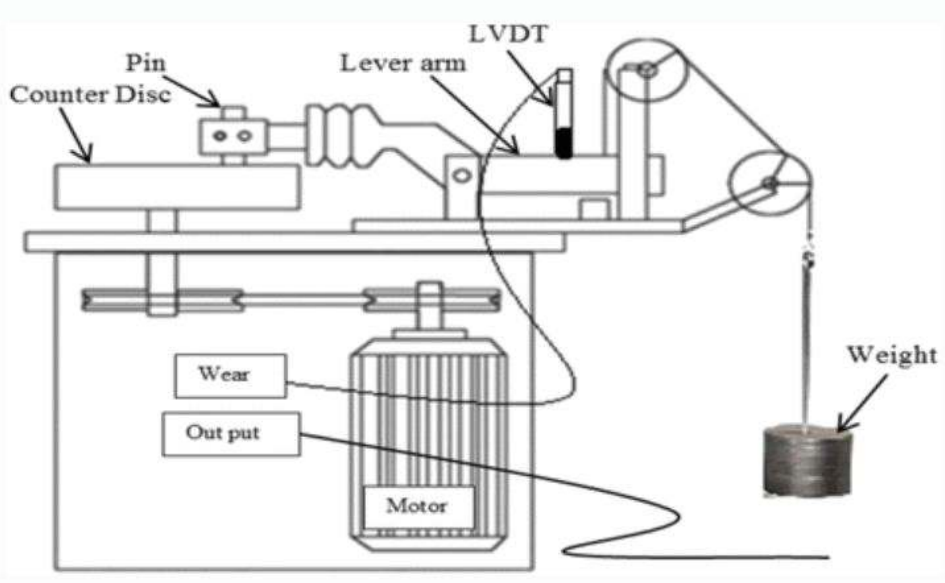

FIGURE 3.11: Schematic Layout of Pin on Disc Wear and Friction Testing Machine [106].

a motor driven spindle, chuck, and a lever-arm device. Chuck holds the revolving disc and lever arm is used for the specimen to force against the revolving disc specimen at a constant load. Speed motor works at a constant speed under load, and this should be mounted carefully so that its vibration does not affect the experiment. The stationary

specimen holder is used for holding the pin specimen, which is attached to the lever arm. The applied load, the speed of disc rotation and other parameters are variables which can be varied, depending on the material to be tested.

Wear loss is calculated by measuring the material loss in volume (mm^3) per unit relative distance traveled (km). Linear wear loss can also be estimated by measuring the mass loss of the material using a high sensitivity balance. Following steps are used for the wear measurement:

1) For the wear measurement, the pin shape or ball shape specimen is placed on a flat circular disc. The motion of either flat disc or pin specimen causes the slide motion between both the surfaces. The disc plane may be oriented vertically or horizontally depending upon the test requirements.

2) The pin specimen is forced on the flat and smooth disc at normal applied load with the help of lever and attached weights. Pneumatic or hydraulic methods can also be used.

3) Wear results in the form of volume loss in mm^3 for the test specimen and disc. Two different materials can be tested by testing each material in both the pin and disc positions.

4) The wear loss is determined by measuring the linear dimensions of the specimens before and after the test. This can also be done by measuring the difference in weight after the test. The loss in mass value is converted to volume loss (in mm^3) using the specimen density value.

5) Wear test is performed for a specific sliding distance, load, and speed. Wear results can be represented as a plot between wear loss and sliding distance. The obtained plots

may show non-linear relationships between wear volume and distance for certain duration and then linear behavior for rest of the duration.

In our work, a dry sliding wear test was conducted using a pin on disc wear testing machine purchased from Magnum Engineers, Bangalore, India. Specimens in cylindrical pin form (12 mm diameter) were used for testing. Grinding of the disc (hardened steel disc with a hardness of HRC 60) was done using an alumina wheel, and polishing was done with the help of different grades of emery papers to make the surface plain. The surface of the pin to be examined was also polished using emery papers, cleaned and weighed before the test. No gap or tilt between the disc and specimen surface was allowed during the test. The test was conducted at sliding velocity as 4 m/sec performed for 1h. For alloy specimens, the wear characteristics were studied under a normal applied load of 5N, 10N and 20N. For composite specimens, the test was performed and studied under applied load 10, 20 and 30N. Two readings were taken for each load. The weight loss of the alloy and composite pins were measured at intervals of 1h using an analytical balance having 0.0001g accuracy. Wear rate was calculated by using the total volume loss occurred in pin specimen during the test.

3.3.6 Corrosion

The test was performed on an SP-150 Biologic electrochemical cell having three electrodes connected to Biologic Instrument Potentiostat/Galvanostat. Fig. 3.12 shows the schematic of experimental set up used for corrosion test. It includes a potentiostat, three electrodes cells and a monitor for recording the data. The exposed surface of the specimen

was used as a working electrode, platinum electrode as an auxiliary electrode, and standard Ag-AgCl was used as a reference electrode. Fig. 3.13 shows three neck cell used for electrode mounting during the test. Each part of the cell is mentioned in this schematic.

FIGURE 3.12: Schematic Layout of experiment setup used for corrosion test.

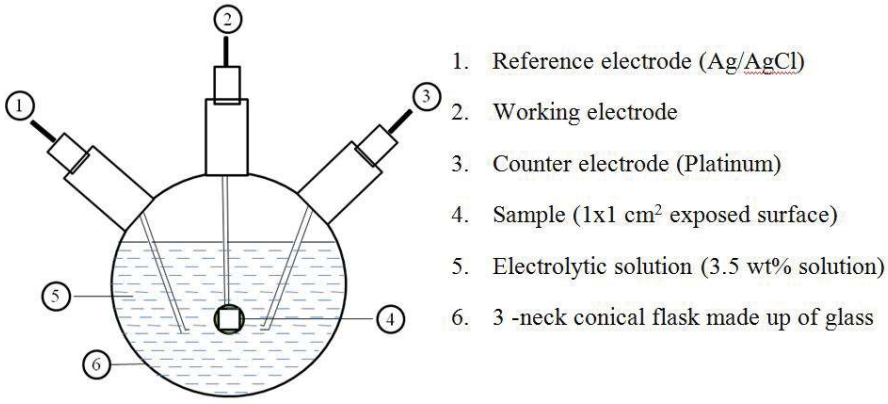

FIGURE 3.13: Schematic of the three neck cell used for electrodes mounting.

• **Coupon Preparation:** 3 mm thick disc of the prepared specimen was taken and abraded using different grade emery papers and diamond paste. They were then properly cleaned by ultrasonication in acetone medium for 5 minutes. 1x1 cm^2 surface area of the dried specimen was exposed for the corrosion test, whereas remaining surface was completely coated by using protective nail paint.

• **Electrolytic solution:** Electrolytic solution of NaCl was prepared by dissolving 3.5wt.% NaCl in distilled water. 150 ml volume of the electrolyte was taken for each experiment.

• **Potentiodynamic Polarization Measurements:** Before starting measurements, the electrodes were kept in electrolytic solution for around one hour to get stabilized and to obtain open circuit potential (OCP). Potentiodynamic polarization curves were recorded with respect to OCP in the range -250 to +250mV at a scan rate of 0.5 mV/s. Corrosion

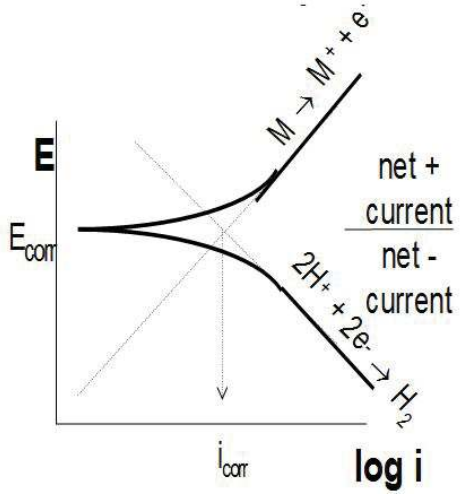

FIGURE 3.14: Tafel extrapolation technique for finding corrosion parameters [107].

current density (I_{corr}) and Corrosion potential (E_{corr}) were calculated by extrapolating the cathodic and anodic linear segments of the Tafel plots to the intersection point. Protection efficiency has been obtained by using respective I_{corr} values. The extrapolation of both the regions are explained according to the Fig. 3.14. Corrosion rate is calulated with the help of I_{corr} value obtained from Tafel plots using the formula:

$$C_r(mpy) = \frac{0.13 I_{corr}(E.W.)}{d} \tag{3.1}$$

• **Electrochemical Impedance Spectroscopy (EIS):** Electrochemical impedance spectroscopy (EIS) measurements were performed at 5 mV AC signals in a frequency range from 100 kHz to 0.01 Hz at OCP. EC lab software was used for the analysis of obtained impedance plots. The nyquist plots obtained from the EIS measurement can be

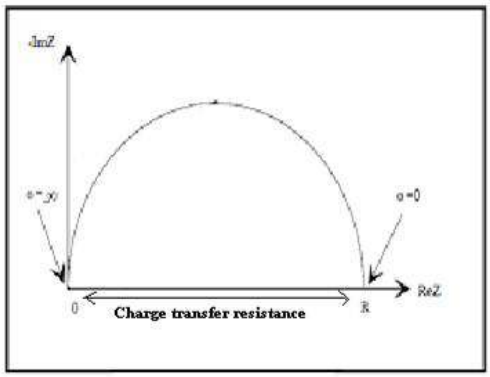

FIGURE 3.15: Nyquist plot [108].

understood from Fig. 3.15. Charge transfer resistance values can be calculated from the difference in the impedance at lower and higher frequencies. One can access the rate of corrosion from the charge transfer resistance. Higher charge transfer resistance shows lower corrosion rate. When multiple charge transfer processes responsible for corrosion are operating, then two or more semicircles are observed in nyquist plots. This can be observed in case of composite materials. Each transfer process is represented by its RC equivalent circuit model.